JOURNAL OF MATERIALS SCIENCE **36** (2001) 4977 – 4987

Formation and evaluation of highly uniform aluminate interface coatings for sapphire fiber reinforced ceramic matrix composites (FRCMCs) using carboxylate-alumoxane nanoparticles

RHONDA L. CALLENDER, ANDREW R. BARRON*
Department of Chemistry and Department of Mechanical Engineering and Materials Science, and Center for Nanoscale Science and Technology, Rice University, Houston, Texas 77005, USA
E-mail: arb@rice.edu; url: www.rice.edu/barron

Sapphire fibers have been dip-coated in aqueous and $CHCl_3$ solutions of carboxylate-alumoxane nanoparticles and calcium-, lanthanum-, and yttrium-doped carboxylate-alumoxane nanoparticles and fired up to 1400°C to form uniform, conformal and contiguous, aluminate coatings. Optimum solvent, dip/dry, and firing sequences were determined for the formation of crack-free coatings. Both carboxylate-alumoxane and ceramic coated fibers were examined by field emission scanning electron and transmission electron microscopy, microprobe analysis and optical microscopy. Coatings produced were stable to thermal cycling in air up to a temperature of 1400°C. The ability of the carboxylate-alumoxanes to provide crack infiltration and repair was demonstrated. Sapphire fiber/alumina matrix FRCMCs have been prepared with calcium-, lanthanum-, and yttrium-aluminate interphase layers. Microscopy and fiber push-out data confirm that the calcium- and lanthanum-aluminate coatings provide a means for controlling failure properties at the fiber-matrix interface. However, FRCMCs containing YAG-coated fibers failed catastrophically before interfacial debonding and/or sliding occurred.

1. Introduction

Were it not for their disposition to brittle fracture, many ceramic materials would be ideal candidates for use in high temperature and severe stress applications, such as next-generation automobile components and aircraft gas turbine engines [1]. Fiber-reinforced ceramic matrix composites (FRCMCs) can be reduced or eliminate catastrophic brittle failure by providing various mechanisms that dissipate energy during the fracture process. The operation of toughening mechanisms depend, to a large extent, on the degree of chemical and/or mechanical bonding at the fiber-matrix interface [2]. A major drawback in existing FRCMCs is the absence of a fiber-matrix interface or interphase that is weakly debonding but stable over the entire range of expected use. The fiber-matrix interface must be sufficiently weak to allow debonding and sliding when a crack impinges upon it, otherwise the crack passes through the fiber and there is minimal or no toughening. Hence, control of interfacial properties has become a key factor in developing FRCMCs and predicting overall composite behavior. Since the choices of fiber and matrix are limited, chemically designed interlayer coatings that can be used to optimize the mechanical properties of the interface are being investigated. The function of the interlayer is to prevent deleterious chemical reactivity between the fiber and matrix as well as protecting the fibers during processing, fabrication, and use [3, 4]. In addition, it must have sufficient apparent shear strength for load transfer but also be weak enough to debond or slip when close to a propagating crack [3–5]. Such interlayer coatings would provide a mechanism for manipulating the graceful versus catastrophic failure of FRCMCs.

Alumina-based materials currently dominate the engineered ceramics and ceramic composites markets due to a combination of excellent physical properties and the relatively low cost of raw materials. Oriented single-crystal alumina (sapphire) fibers exhibit excellent thermomechanical properties and have the distinct advantage over their non-oxide competition of being innately stable with respect to oxidation at high temperature. Although matrix cracking is minimized due to the match in thermal expansion of alumina fiber the possibility for chemical bonding and the chemical reactivity of the interface has limited the application of sapphire-fiber/alumina matrix composites. The standard solution for this problem is to employ coatings that are phase compatible with both the aluminum oxide fiber

*Author to whom correspondence should be addressed.

and matrix [6]. An alternative approach has been proposed by Cinibulk [7] and Morgan and Marshall [8] in which the interlayer inherently provides a means to influence interfacial debonding behavior. In this approach, the fiber is coated with a layered material having easily cleaved crystallographic planes oriented in such a way as to promote deflection of matrix cracks away from the fiber. A group of materials with high temperature stability and the required crystallographic planes are the mixed aluminates with β-alumina and magnetoplumbite type structures, e.g., calcium hexaluminate ($CaAl_{12}O_{19}$, the mineral hibonite) and the structurally similar lanthanum hexaluminate ($LaAl_{11}O_{18}$) [9].

Magnetoplumbites consist of layered spinel blocks $[Al_{11}O_{16}]^+$ with stabilizing cations and oxygen anions in the interspinel layer [10, 11]. The magnetoplumbites hibonite and lanthanum hexaluminate are stable up to about 1800°C and have been shown to be thermochemically stable with alumina. However, phase formation is reported to be very slow [12], and smooth, homogeneous interlayers have been difficult to achieve via sol-gel methods without the presence of significant Al_2O_3 and $LaAlO_3$ impurities [13].

Thin oxide coatings on fibers have traditionally been produced by either chemical vapor deposition or by sol-gel. Despite the relative simplicity of the sol-gel process, careful control over a large number of parameters is required to obtain uniform coatings without significant surface cracking [14]. Thus, the development of such methods to form uniform coatings which are functional interlayer materials in FRCMCs is desirable. The goal of our research is the development of a low cost and highly flexible synthetic methodology and compatible processing techniques for the fabrication of interlayer coatings and subsequent composite materials. We propose to accomplish this goal through the use of a unique class of flexible materials: chemically functionalized alumina nanoparticles: carboxylate-alumoxanes.

Carboxylate-alumoxanes are aluminum oxygen nanoparticles with a boehmite-like core structure and an organic periphery [15], that are readily prepared by reaction of boehmite, $[Al(O)(OH)]_n$, with carboxylic acids (HO_2CR where R is an organic group) [16]. Specifically, the use of polyether substituents [e.g., methoxy (ethoxyethoxy)acetic acid, MEEA-H, $HO_2CCH_2O(CH_2CH_2O)_2CH_3$] and methoxy(ethoxy)acetic acid, MEA-H, $HO_2CCH_2OCH_2CH_2OCH_3$] allows for their synthesis in aqueous media which enables environmentally benign processing [15, 17]. Unlike traditional sol-gels, the alumoxane precursors are infinitely stable in both solid and solution. While the parent alumoxanes yield alumina upon thermolysis, we have demonstrated that reaction of the carboxylate-alumoxane with a metal acetylacetonate complex, $M(acac)_n$, results in transmetallization and the formation of a metal-doped carboxylate-alumoxane [18, 19]. Upon thermolysis the metal-doped carboxylate-alumoxanes form homogenous mixed metal oxides with high phase purity (including aluminates) at reduced temperatures [20]. Another consequence of atomic scale mixing is that crystal growth occurs after phase formation, an effect further enhanced by the nano-size of the carboxylate-alumoxane particles. Given these advantages, we propose that carboxylate-alumoxane materials and methodology have potential in the development of a low cost and highly flexible synthetic approach for the fabrication of composite materials.

2. Experimental procedure

2.1. General

Research grade boehmite (Catapal B) was provided by Vista Chemical Company. All carboxylic acids and metal acetylacetonate complexes (Aldrich and Fluka) were used without further purification. Methoxyacetate-alumoxane (MA-alumoxane), methoxyethoxyacetate-alumoxane (MEA-alumoxane), methoxy(ethoxyethoxy) acetate-alumoxane (MEEA-alumoxanes), and yttrium-, calcium-, and lanthanum-doped carboxylate-alumoxanes were prepared by previously published methods [18, 20].

Field emission scanning electron microscopy (FESEM) studies were performed on JEOL 6320F microscope. Analyses of samples in cross-section specifically addressed the thickness of the coating. The optical thickness and uniformity of coatings were evaluated by observing color shifts in the Fizeau interference fringes in white light over the length of the monofilament using reflected light optical microscopy [21]. A uniform coating was defined as one that showed no discernible thickness differences and an absence of inhomogeneities such as bubbles or precipitates over the length of the fiber. Electron probe microanalysis (EPMA) was performed on a Cameca SX50 Electron Microprobe using techniques and imaging modes including: energy dispersive X-ray spectroscopy (EDS), secondary electron emission (topography, morphology), back scattered electron emission (atomic number contrast), X-ray emission (quantitative analysis and element distribution mapping), and cathodoluminescence (trace element distribution). In addition, wavelength dispersive X-ray distribution maps (i.e., elemental maps) were used to determine the compositional homogeneity of the coatings. The following microprobe calibration standards were used: CaO (Ca), corundum Al_2O_3 (Al), quartz SiO_2 (O), and rare earth (RE) element orthophosphates $(RE)PO_4$ (Y, La). The tensile strength of coated fibers was determined using a MTS 858 MiniBionix Instrument. Samples were evaluated at room temperature under fast fracture conditions with 0.25 inch (0.625 cm) gage lengths. The crystallographic structure of the coatings was most readily determined by X-ray diffraction (XRD) analysis of samples sintered alongside, and in an exactly analogous manner to, the fiber samples. All XRD data were collected on a Siemens Diffractometer (B).

2.2. Fiber coatings

Prior to use, single-crystal c-axis-oriented α-Al_2O_3 (i.e., sapphire) fibers, *ca.* 140 μm in diameter (Saphikon, Inc., Milford, NH), were cleaned with acetone and/or dilute HCl. Coatings were prepared by dipping the cleaned fibers into a 2, 6, 12, or 20 wt% $CHCl_3$ or H_2O solution of the metal doped carboxylate-alumoxane and drying using a heat gun, in a low temperature oven (i.e., 55°C), or at room temperature. Repeated dipping/drying was performed until the desired

coating thickness (0.1–6.0 μm depending on application) was obtained. The samples were thermally processed by one of the following ways: (a) the sample was heated from 25°C to 500°C and held for 2 hours; (b) the sample was heated from 25°C to 500°C and held for 2 hours, followed by a temperature ramp ($10°C \cdot min^{-1}$) to a maximum temperature of 1400°C which was then maintained for a minimum of 2 hours; (c) the sample was heated in a single step from 25°C directly to a specified maximum temperature at $55–75°C \cdot min^{-1}$.

2.3. Fabrication of FRCMC flexure bars using an alumoxane matrix

MEEA-alumoxane and MA-alumoxane were prepared per previously reported methods [15]. A 1 : 1 physical mixture of MEEA-A : MA-A was synthesized by adding MEEA-alumoxane (5.0 g) and MA-alumoxane (5.0 g) to 150 mL water and stirring at room temperature for 30 min. The water was evaporated *in vacuo* and the resulting solid was dried at 55°C to a fine white powder for storage. As needed, an aqueous solution of the preceramic nanoparticles was prepared whereupon the water was slowly evaporated by stirring on a hot plate to form an inviscid gel, which was used as the matrix material in FRCMC fabrication. Thermal processing of composite samples was accomplished as follows: (a) the sample was heated in a furnace at the rate of $5°C \cdot min^{-1}$ for thermal ramps from 25 to 200°C, and 500°C to the indicated maximum temperature ($T_{max.}$); during the intermediate thermal ramp from 200 to 500°C, the rate was decreased to $1°C \cdot min^{-1}$, to minimize possible cracking of the coating. The sample was sintered at $T_{max.}$ for a dwell time ranging from 6 to 24 h, depending on the application; (b) the sample was cured at 55°C for 2 h. in a laboratory oven, then transferred to a furnace preheated to 55°C. The sample was then processed per the ramp/soak series in method (A) with exception that the initial temperature was 55°C in the first ramp step.

2.4. Hot press fabrication of flexure bars

The coated sapphire fibers were pressed in a matrix of alumina powder (spray dried 99.9% α-Al_2O_3, Coors, Golden, CO) under 5–10 ksi (34–68 Mpa) pressure using a 4 mm × 50 mm rectangular die, followed by firing in air at 1660°C for 2 hours. The fibers were placed parallel to the long dimension and in the middle of the bar. The flexure bars displayed a density of about $3.90\ g \cdot mL^{-1}$; this is the expected density for this composition ($3.98\ g \cdot mL^{-1}$) and meets the minimum industry standard of $3.88\ g \cdot mL^{-1}$. The porosity was all closed except perhaps around the fibers. There was some distortion of the bars due to the approximately 20% linear dimensional shrinkage of the matrix during sintering; the fibers did not sinter or shrink. No cracking of the matrix was observed.

3. Results and discussion

Conditions for the preparation of uniform fiber coatings using water soluble carboxylate-alumoxane nanoparticle precursors were investigated. All of the metal-doped carboxylate-alumoxane coatings (i.e., pre-fired) and converted aluminate coatings (i.e., post-fired) were characterized with respect to coating morphology, and structural orientation. The crystallographic structure of the coatings was most readily determined by XRD analysis of powdered samples sintered alongside the fiber samples. In all cases phase identity was confirmed [20].

Sapphire monofilament fibers were coated by dipping with a draw speed of 1–5 $cm \cdot s^{-1}$ into a reservoir containing a water or chloroform ($CHCl_3$) solution of metal-doped carboxylate-alumoxane concentrations varying from 2–20 wt%. Water and chloroform solvents were chosen for comparison because while water allows for environmentally sensitive processing, it is slow to evaporate, whereas $CHCl_3$ evaporates rapidly (bp = 61°C). No discernible difference was noted between coatings formed from $CHCl_3$ or H_2O solutions despite the difference viscosities of these solvents, 0.542 and 0.8904 cp, respectively [22]. The H_2O solutions with higher wt% concentrations were dried slightly longer between dips, otherwise the coating would redissolve during subsequent dipping or form bubbles during final heat treatment. Upon conversion to ceramic, the choice of solvent appeared to have no effect on the microstructure of the aluminate coating. The post-sintered coating thickness (0.1–6.0 μm) was found to depend on the concentration of the metal-doped carboxylate-alumoxane solution and, to a lesser extent, the draw speed. Coating thickness can be controlled by careful variation of these processing conditions whereby the solution concentration and the solvent are taken into consideration in a manner similar to traditional sol gel [23]. A linear relationship between number of dips and final ceramic coating thickness is depicted in the plot shown in Fig. 1. In all cases the coatings were found to be within 10% along the entire length of the coated fiber. Any variation may be traced to the variability in the draw speed since this was performed manually.

Processing prior to final sintering involved drying by various methods. If shorter processing times were desired, the use of a hot air gun or oven drying could be employed. Rapid drying did not unduly influence the quality of the coating for the aqueous processing,

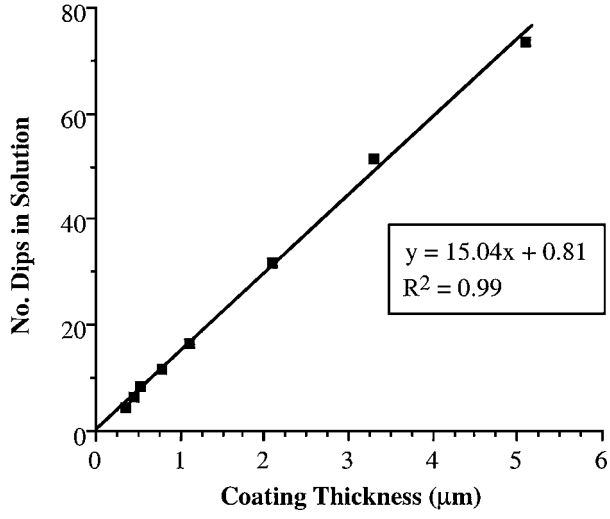

Figure 1 Plot of number of dips in solution versus ceramic coating thickness, showing thickness increasing linearly with multiple dips in 6 wt% carboxylate-alumoxane solution.

although due to the high volatility of the solvent it was found that the use of a hot air gun with $CHCl_3$ solutions resulted in cracking of the fiber coating. These coatings could, however, be fully repaired by additional dip/dry cycles. It was also found that laying the "wet" coated fibers on a surface caused adherence to the contact area during drying, resulting in damage to the coating when it is removed from the surface. However, once dried, no subsequent damage resulted from general contact between coated fibers and surfaces. Formation of aluminate coatings on sapphire fibers was accomplished by thermal conversion in air to temperatures between 1000–1400°C. Conditions for conversion of metal-doped carboxylate-alumoxane nanoparticles to ceramic materials have been reported elsewhere [20].

In order to investigate the trends and allow for comparisons with previously characterized materials and synthetic methods, the following discussion is divided according to the aluminate ceramic coating. Calcium hexaluminate (hibonite) and lanthanum hexaluminate were expected to provide successful debonding due to their inherantly weak cleavage planes. Conversely, YAG was chosen as a control, since although it has a similar thermal expansion ($\alpha = 8.9 \times 10^{-6\circ}C^{-1}$) [24] to alumina, it is not inherantly weak, and does not have oriented layers to allow for debonding at a fiber/matrix interface.

3.1. Calcium hexaluminate

The surface of Ca-doped MEEA-alumoxane coated sapphire fiber (prior to sintering) is shown in the SEM image in Fig. 2a. The absence of surface cracks or discontinuities results in a smooth morphology and conformable topography. The corresponding elemental maps (Fig. 2b and 2c) confirm the chemical identity and show the uniform distribution of Al and Ca in the coating. Similarly, the surface of Ca-doped MEA-alumoxane coated sapphire fibers are also uniform and free of surface defects. The Ca:Al ratio as measured by EDX were found to vary between samples due to "see through" of the underlying sapphire fiber. However, no variation was found along the fiber length. Furthermore, powdered samples of the appropriate alumoxanes were sintered adjacent to the coated fibers and these samples were analyzed by XRD and EDX confirming the identity of the crystalline phase: $CaAl_{12}O_{19}$ (JCPDS #38-0470) [20].

All of the calcium hexaluminate coatings were found to be conformal and contiguous with no significant surface flaws as indicated by FESEM and optical microscopy analyses. As a representative example, the hibonite coating from thermal conversion of Ca-doped MEA-alumoxane is shown in Fig. 3. The lack of any surface features, the invariance in the coating thickness over the entire length of the sample, and the EPMA

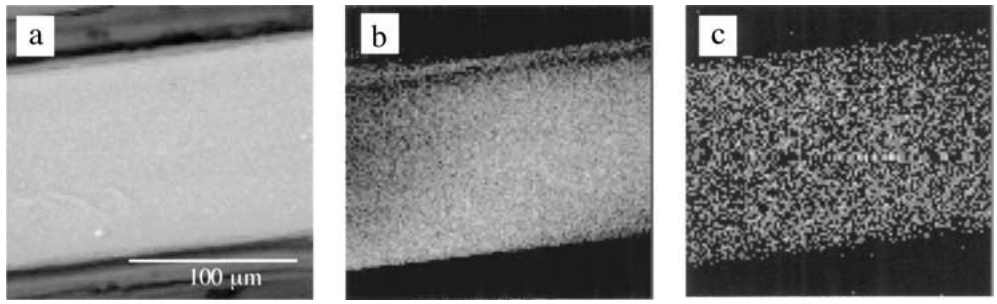

Figure 2 SEM image (a) and associated two-dimensional Al (b) and Ca (c) X-ray elemental maps of a Ca-doped MEEA-alumoxane coated sapphire fiber formed from a 6% aqueous solution dried in air.

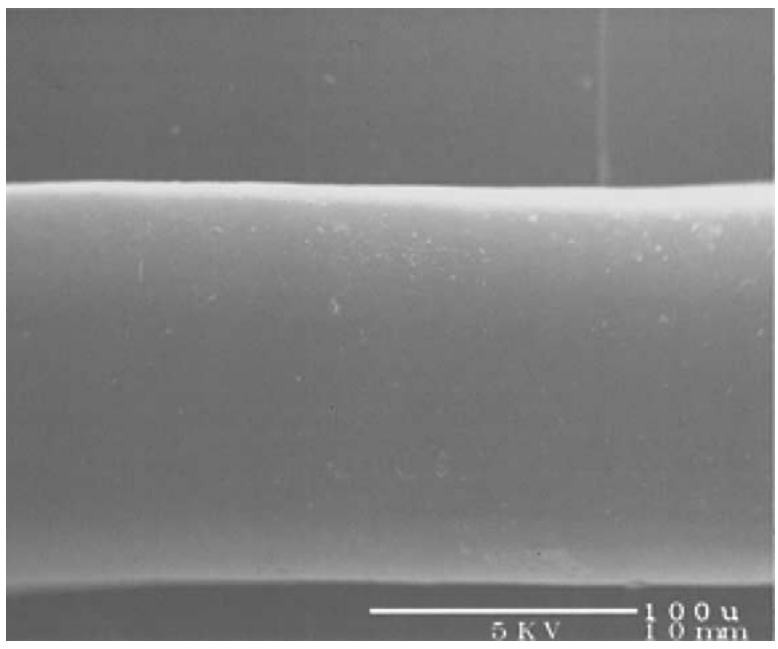

Figure 3 FESEM image of a $CaAl_{12}O_{19}$ coating on a sapphire fiber resulting from a 6% aqueous solution of Ca-doped MEA-A.

elemental maps each confirmed the uniformity of the aluminate coating. Since calcium diffusion from the coating has been reported to cause fiber embrittlement and coating degradation [25], EPMA and optical microscopy were also used to determine Ca : Al ratios for the surface of the coatings. The Ca : Al ratios determined by EDS before and after firing were found to be consistent, indicating minimum diffusion of calcium into the fiber.

It has been suggested that the morphology of a fiber coating will significantly effect the interphase stability under fracture and/or shear conditions [3]. Features which are considered detrimental include spallation and peel back of the coating. Notably, the aluminate coatings shown in the figures above are highly uniform, with no evidence for bridging or peel back on either pre- or post-fired fibers. This is confirmed for all Ca-doped samples formed from thermolysis of doped carboxylate-alumoxane nanoparticle coatings on sapphire fibers. High resolution FESEM images of the surface of the ceramic coating indicate its polycrystalline nature (Fig. 4). The crystallite size ranges from 60–70 nm based on FESEM point to point measurements; confirmed by XRD measurements. While a few pinholes (or divots) appear in the hexaluminate surface, it is not clear that they occur through to the fiber surface.

The FESEM images of calcium hexaluminate coated fiber after the coating has been physically broken are shown in Fig. 5. Several important observations may be made from this (and similar) images. First, the hexaluminate coatings appear to have a layered texture and microstructure characteristic of the magnetoplumbite-type structure. Second, debonding of the coatings and cleavage occurring within the hibonite layers are

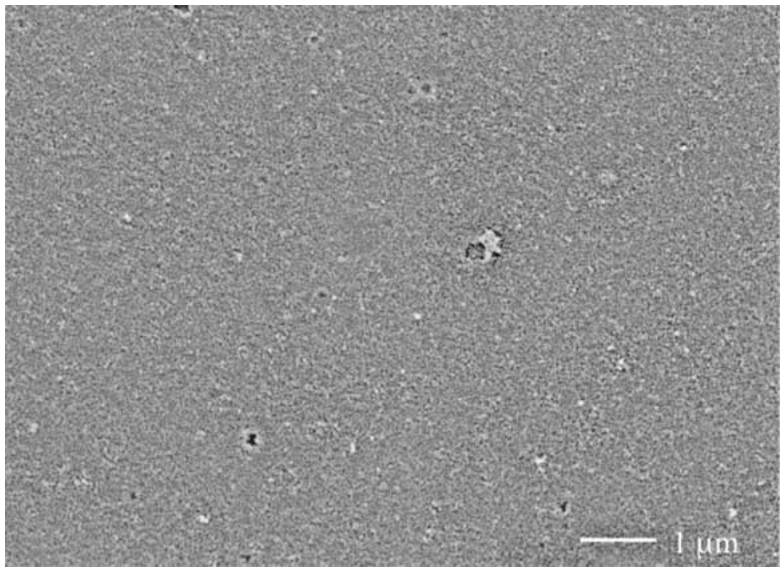

Figure 4 High resolution FESEM images of the surface of a $CaAl_{12}O_{19}$ coated sapphire fiber formed from a 6% $CHCl_3$ solution of Ca-doped MEEA-A.

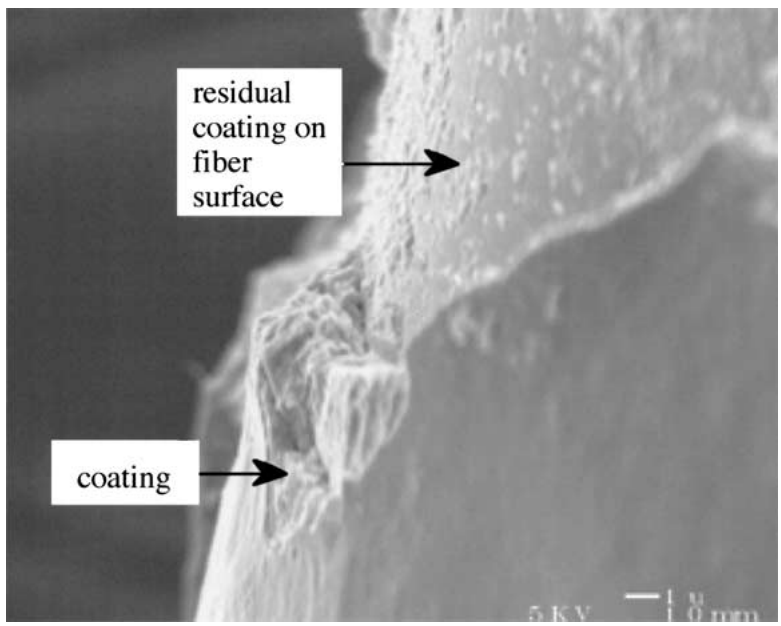

Figure 5 FESEM images of $CaAl_{12}O_{19}$ coated sapphire fibers after fracturing to evaluate the fiber-coating interface. The coating was prepared by the thermolysis (1100°C) of a Ca-doped MEEA-A coating prepared from a 6% aqueous solution.

observed as primary modes of fracture. This is desirable, and suggests the advantageous orientation of crystallographic basal planes parallel to the fiber axis. Finally, where the coating has spalled away from the fibers significant debris remains on the fiber surface, indicating that the adhesion failure occurring within the coating is at least equal to that at the interface. The presence of calcium hexaluminate on the fiber surface was confirmed by EDX analysis.

The filament strength of "bare" sapphire and hibonite coated fiber samples was measured at room temperature to confirm the benign nature of the coating process on innate fiber strength. Previous studies [7, 8] have shown that fiber degradation is often caused by morphological instability of the interface, due to grain growth during fabrication and high temperature annealing. However, no significant reduction in tensile strength was observed for fiber samples coated with hibonite derived from Ca-doped alumoxane nanoparticle solutions even after sintering to 1500°C for 2 h. Reproducible values in the range 2.4–2.7 GPa were obtained, consistent with bare fiber measurements (2.3–2.7 GPa) and commensurate with manufacturer specified strengths (2.5–2.9 GPa).

3.2. Lanthanum hexaluminate

The appropriate metal stoichiometry for $LaAl_{11}O_{18}$ coating composition was determined from EDS elemental line scans, while the phase purity (JCPDS #33-0699) was confirmed by XRD [20]. SEM images and corresponding elemental maps reveal the smooth, continuous nature and homogeneous metal distribution of the lanthanum hexaluminate coating.

In order to investigate effects such as processing stability and thermal stress on alumoxane-derived aluminate coatings, a lanthanum hexaluminate coated fiber was subjected to repeated thermal cycling in air at temperatures where structural FRCMCs are likely to be

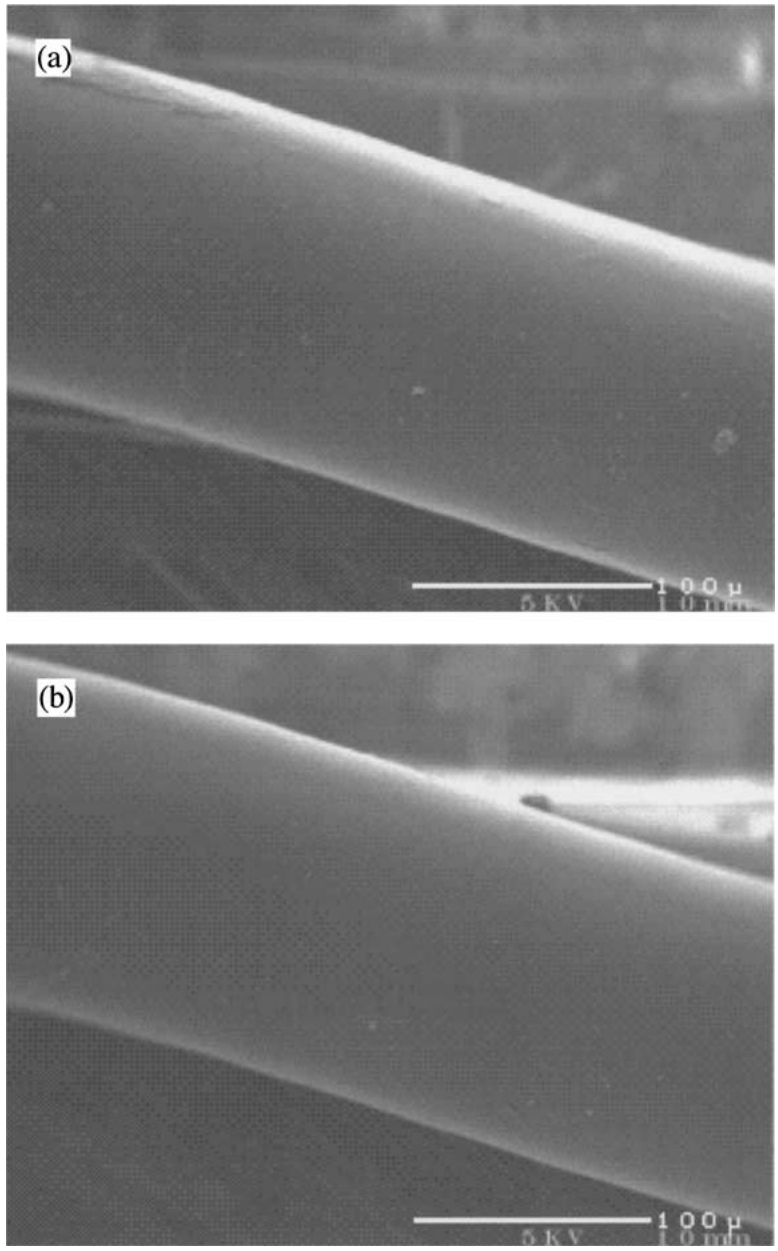

Figure 6 FESEM images of a $LaAl_{11}O_{18}$ coated sapphire fiber, pre (a) and post (b) thermal cycling 4 × 1400°C. The coating was prepared by the thermolysis (1100°C) of a La-doped MEEA-A coating prepared from a 6% aqueous solution.

used. The sample was initially processed per standard parameters, followed by four consecutive thermal cycles consisting of a single-step temperature ramp from room temperature to 1400°C in air. The sample was allowed to return to room temperature between each cycle. FESEM images of the sample are shown prior to firing and following the final thermal cycle in Fig. 6. As can be seen in Fig. 6b, the coating surface remained very uniform following thermal cycling. In fact, there appear to be no discernible changes in the composition, smoothness or adherence of the coating as compared to thermal cycling in air.

Some samples were damaged due to processing conditions or severe handling, which presented an opportunity to evaluate the repair capability of carboxylate-alumoxane nanoparticle solutions. Although fiber coatings cannot be repaired within a composite structure, there is interest in the repair of surface damage due to handling or processing. A damaged $LaAl_{11}O_{18}$ coated sapphire fiber is shown in Fig. 7a. The sample was readily repaired by repeatedly dipping in 12 wt% $CHCl_3$ solution of lanthanum-doped carboxylate-alumoxane nanoparticles followed by calcination to 500°C in air (Fig. 7b). Although the repaired areas are apparent, there is no indication of cracking, peeling, or spallation and the surface is relatively uniform despite the thick (*ca.* 4.5 μm) coating. The damage repair was confirmed as well by microprobe analysis. WDS analysis indicated that a homogeneous metal distribution over the repaired areas.

The filament tensile strength of lanthanum hexaluminate coated fiber samples was measured at room temperature. Consistent measurements in the range 2.3–2.5 GPa were obtained for samples after sintering to 1400°C for 2 h., confirming the benign nature of the coating process on innate fiber strength.

3.3. Yttrium aluminum garnet

Yttrium aluminum garnet (YAG, $Y_3Al_5O_{12}$) coatings on sapphire fibers were produced by thermolysis

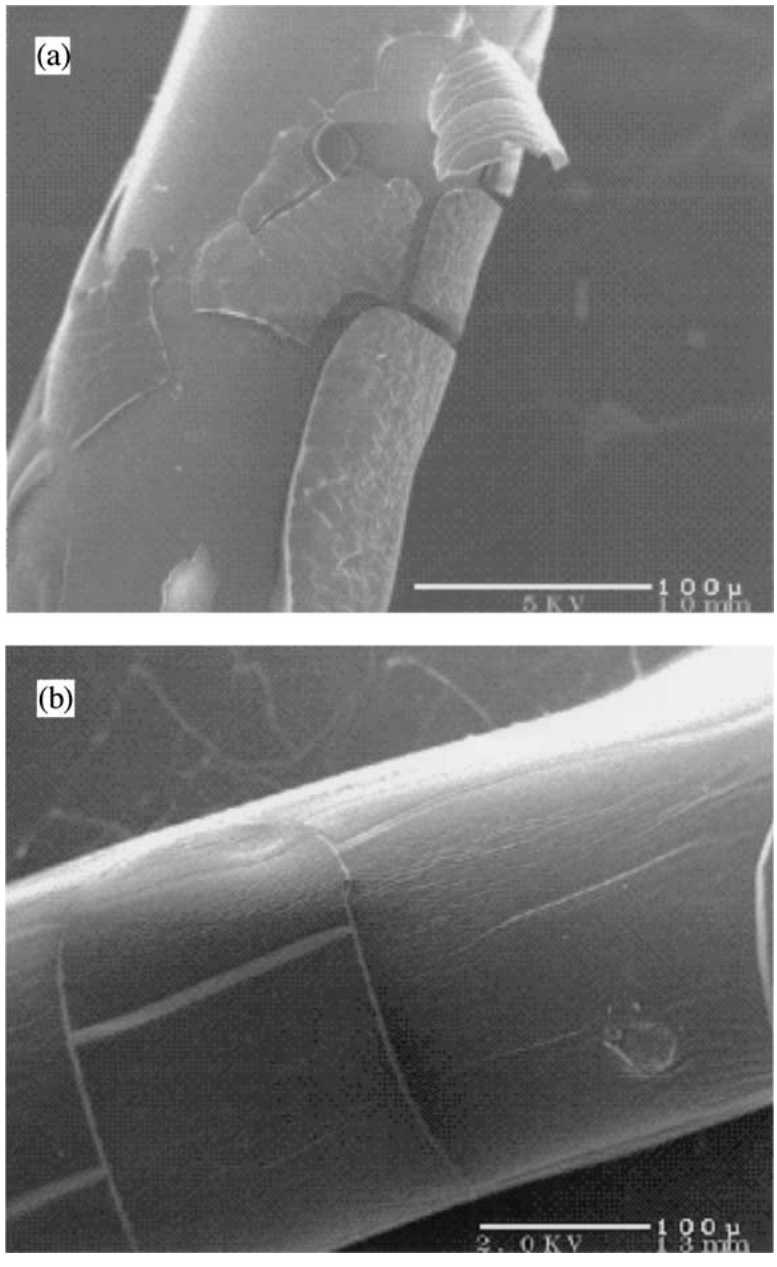

Figure 7 FESEM images of a (a) damaged and (b) repaired $LaAl_{11}O_{18}$ coated sapphire fiber.

of yttrium-doped carboxylate-alumoxane nanoparticle precursors. Phase formation (JCPDS #33-0040) and elemental composition were confirmed by XRD and EDX, respectively [20]. All drying and sintering environments using aqueous solution precursors resulted in smooth, continuous, adherent coatings. However, chloroform solutions with high wt% concentrations of yttrium-doped carboxylate-alumoxane nanoparticles showed spalling and peeling of coatings upon thermolysis. This effect was especially pronounced with sapphire fibers which were not cleaned prior to coating. Although the solution wetted the surface, the coatings did not bond well upon firing and tended to curl and peel off. Spallation also occurred when combined with drying by heat gun airflow. The onset of such is believed due to the excessive drying rate in this case, where the warm air from the heat gun contributed to the already high volatility of chloroform. This caused rapid evaporation of volatiles and the coating was likely dried before it had time to adhere to the substrate. However, as discussed previously, even extremely damaged specimens were readily repaired using appropriate conditions.

The results of tensile test measurements on YAG coated fiber samples indicate sapphire monofilament strength was maintained after coating and processing. Values of 2.3–2.4 GPa were obtained, consistent with other aluminate coated sapphire fibers.

3.4. Fiber-reinforced ceramic matrix composites

Composite specimens with alumoxane-derived interlayers were fabricated for analysis of interlayer debonding. A summary of the composite samples prepared is given in Table I.

As shown in Fig. 8, microscopic analysis of sample **C1** (see Table I) following mechanical testing indicates that failure occurred both by debonding at the interfaces as well as by cleavage within the layers of the $CaAl_{12}O_{19}$ coating, whereby residual coating can be observed on the fiber surface. This mode of failure is desired for effective load transfer from matrix to fiber [3, 8].

TABLE I Summary of fiber-interlayer-matrix materials and fabrication method employed in FRCMCs

Sample	Reinforcement phase	Interlayer coating	Matrix[a]	Method[b]
C1	Sapphire	$CaAl_{12}O_{19}$	Al_2O_3	Flexure bar
C2	Sapphire	$LaAl_{11}O_{18}$	Al_2O_3	Flexure bar
C3	Sapphire	$Y_3Al_5O_{12}$	Al_2O_3	Flexure bar

[a]Pre-fired matrix material.
[b]Refer to experimental.

Fiber pull-out, push-out and indentation tests have been widely used to measure the interface shear strength and the interface shear stress in a range of fiber-reinforced composites [26–29]. In the present study, fiber push-out tests were performed, on a minimum of 20 fibers for each coating studied, using an indentation technique first proposed by Marshall [30]. A load is applied using a sharp indentor (Vickers pyramid diamond tip) to the center of the fiber, normal to its axis, in a planar section of the composite. A load is applied so that the fiber will slide along the fiber-matrix interface over a distance determined by the force on the indentor. The fiber is therefore elastically compressed by the indentor load over the debonded length, which was assumed to be determined by the interfacial friction. The resulting relationship between the interfacial sliding resistance, τ (also called interfacial friction stress), the force, F, on the indentor, and the distance, u, that the fiber is depressed with respect to the composite matrix surface is shown in Equation 1, where r is the radius of the fiber and E_f is the fiber modulus.

$$\tau = \frac{F^2}{4\pi^2 u r^3 E_f} \quad (1)$$

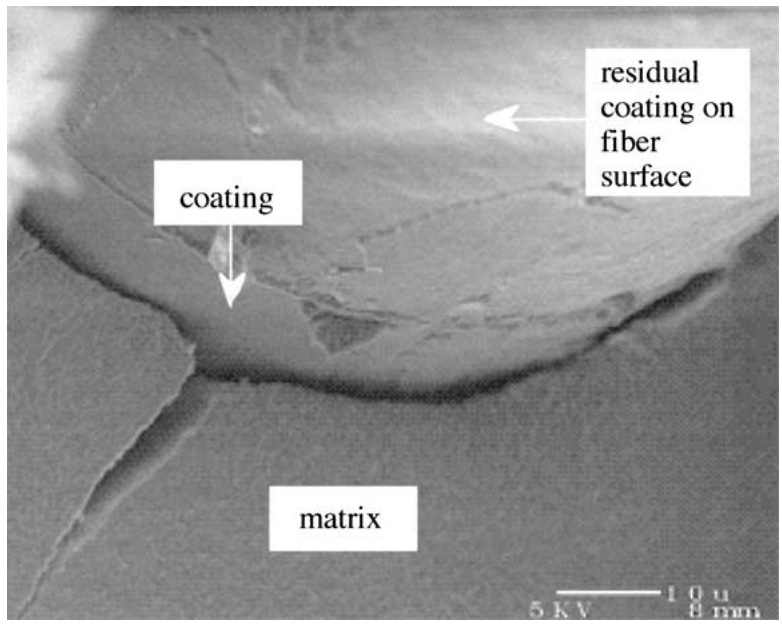

Figure 8 FESEM images of sapphire fiber/alumina matrix composites with hibonite (**C1**) interphase layer after interlayer failure showing the residual coating on the fiber surface.

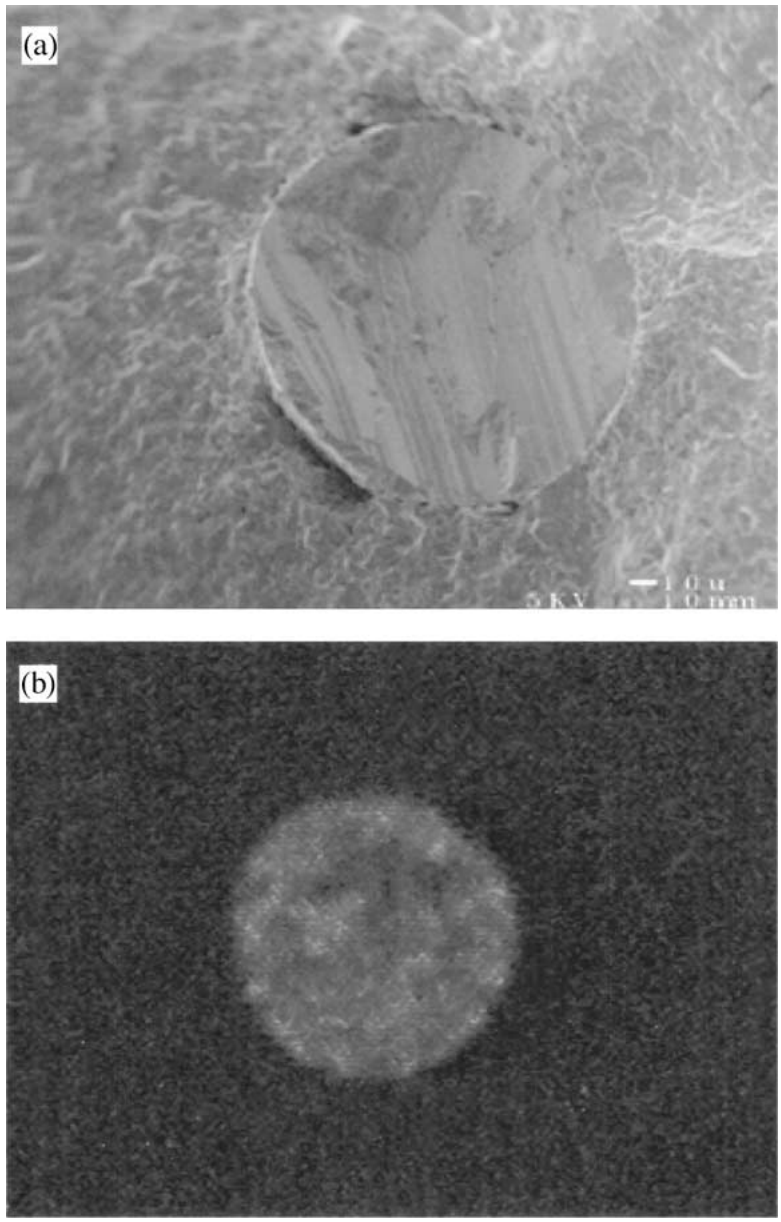

Figure 9 FRCMC (**C1**) consisting of a sapphire monofilament with a hibonite interlayer in alumina matrix, optical micrograph (a) prior to testing and optical micrograph (b) after indentation testing (the after indentation image is back lit for clarity).

If the interface is sufficiently weak, the fiber is expected to debond and slide under the applied force. If the interface is strong, then radial indentation cracks are deflected into the interface layer and the matrix, and possibly also may penetrate into the fiber. Interface systems that satisfy this debond criterion typically have $\tau > 100$ MPa [3, 7, 8].

Composite samples evaluated using this technique included: sapphire monofilament with a hibonite interlayer in an alumina matrix (**C1**), sapphire monofilament with a lanthanum hexaluminate interlayer in alumina matrix (**C2**), and sapphire monofilament with a YAG interlayer in alumina matrix (**C3**). The samples were characterized by FESEM and optical microscopy before and after testing. Both the hibonite (**C1**) and lanthanum hexaluminate (**C2**) interlayers allowed the fibers to slide, indicating that the fiber-matrix interface is sufficiently weak to allow debonding (see, Fig. 9). The frictional sliding resistance calculated using Equation 1 was determined to be 30 ± 10 MPa when the interlayer was hibonite and 25 ± 10 MPa for a lanthanum hexaluminate interlayer. This is within the range expected to be suitable for effective reinforcement of composites [3, 7, 8]. In contrast, high applied loads (up to 120 N) were applied in the presence of a YAG interlayer, which caused many of the FRCMCs to fail catastrophically before interfacial debonding and/or sliding occurred (see Fig. 10). A similar result was obtained for uncoated fibers. In every attempt, ceramic matrix cracking was observed prior to the fiber sliding so that no reproducible results were obtained. Moreover, if values were determined under these high applied loads it is uncertain whether the numbers would actually reflect the interfacial stress, chemical bond strength, or some combination of these and other factors.

The difficulties in pushing out the YAG-coated fibers appeared to be due, in part to high interfacial sliding resistance resulting from interfacial roughness upon debonding [31, 32], or bonding between the coating and the fiber or matrix. The thermal expansion mismatch of

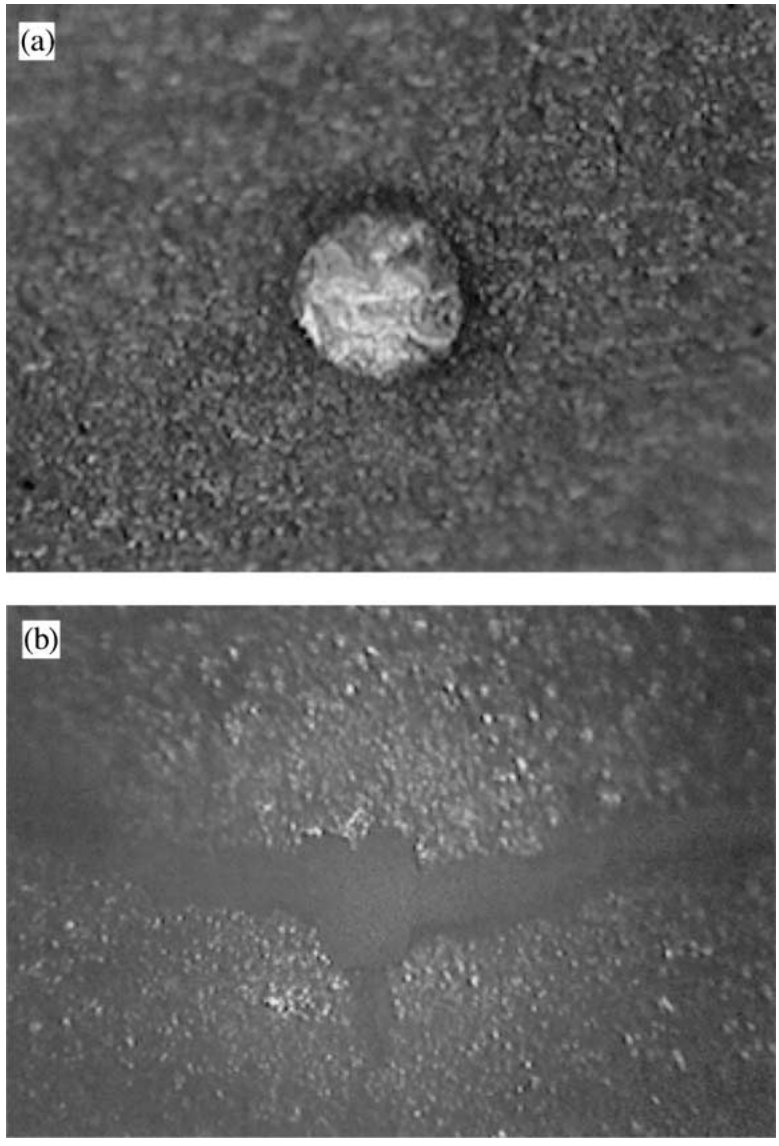

Figure 10 FRCMC (**C3**) consisting of a sapphire monofilament with a YAG interlayer in alumina matrix, FESEM image (a) prior to testing and optical micrograph (b) after indentation testing (the after indentation image is back lit for clarity).

alumina and YAG likely contributed to the high degree of debond roughness, so that even if the fibers debonded they were prevented from sliding due to increased friction [33]. This was evidenced by the observation of radial cracks spreading through the matrix as the fiber was depressed (see, Fig. 10).

4. Conclusions

Yttrium-, calcium- and lanthanum-doped carboxylate-alumoxane nanoparticles may be used as simple, inexpensive, readily processable precursors for hexaluminate and YAG ceramic coatings. Aqueous and chloroform solutions of these carboxylate-alumoxane nanoparticles were found to effectively wet sapphire monofilament fibers and form uniform, conformal, and contiguous coatings over a flexible range of processing (e.g., dipping, drying, etc.) conditions. The long term stability of precursor materials is a key advantage. In addition, the alumoxane methodology allowed for reproducible thickness control as well as proved an effective method to repair cracks and other coating surface damage. Ceramic coatings were stable to temperatures exceeding 1400°C and also during repeated thermal cycling in air at temperatures where structural FRCMCs are likely to be used. No apparent reduction in tensile strength was measured following coating and processing of the sapphire fibers.

The rationale for the use of the lanthanum and calcium hexaluminates as interlayer coatings in FRCMCs was that their layered structure would provide means for controlling failure properties at the fiber-matrix interface. Our push-out data supports this proposal, since the lanthanum and calcium hexaluminate coated fibers performed well on fiber push-out tests. However, FRCMCs containing YAG-coated fibers failed catastrophically before interfacial debonding and/or sliding occurred. Analyses following mechanical failure as well as microstructural investigation of samples with a magnetoplumbite interphase in cross section showed cleavage planes oriented parallel to the surface of the fibers, suggesting that such an interphase is capable of protecting the fiber by deflection of cracks along the easy-cleaving planes. Furthermore, debonding at the fiber-matrix

interface and interlayer sliding of the basal planes were observed as primary modes of failure.

Acknowledgments

Financial support for this work was provided by the National Aeronautics and Space Administration (NASA). The authors gratefully acknowledge Dr. S. Farmer (NASA LeRC) for insightful discussion and for supplying sapphire fibers and Bruce Brinson and Milton Pierson for assistance with FESEM and to EPMA, respectively. We also express appreciation to Cullen T. Vogelson for his helpful suggestions in reviewing the original manuscript.

References

1. "Ceramic Fibers and Coatings: Advanced Materials for the 21st Century," National Materials Advisory Board and National Research Council Commission on Engineering and Technical Systems Publication NMAB-494, National Academy Press, Washington, D.C. (1998).
2. A. G. EVANS and D. S. MARSHALL, *Acta Metall. Mater.* **37** (1989) 2567.
3. R. J. KERANS, R. S. HAY, N. J. PAGANO and T. A. PARTHASARATHY, *Am. Ceram. Soc. Bull.* **68** (1989) 429.
4. R. W. RICE, J. R. SPANN, D. LEWIS and W. COBLENZ, *Ceram. Eng. Sci. Proc.* **5** (1984) 614.
5. R. A. LOWDEN, ORNL/TM-11039, Oak Ridge National Laboratory (1989).
6. J. B. DAVIS, E. BISCHOFF and A. G. EVANS, in "Advanced Composite Materials," edited by M. E. Sacks (American Ceramic Society, 1991) p. 631.
7. M. K. CINIBULK, *Ceram. Eng. Sci. Proc.* **15** (1994) 721.
8. P. E. D. MORGAN and D. B. MARSHALL, *Mater. Sci. Eng.* **A162** (1993) 15.
9. M. K. CINIBULK, *J. Mat. Res.* **10** (1995) 71.
10. A. UTSONOMIYA, K. TANAKA, H. MORIKAWA, F. MARUMO and H. KOJIMA, *J. Solid State Chem.* **75** (1988) 197.
11. N. IYI, S. TAKEKAWA and S. KIMURA, *ibid.* **83** (1989) 8.
12. P. R. C. ROPP and B. CARROLL, *J. Am. Ceram. Soc.* **63** (1980) 416.
13. M. K. CINIBULK, *Ceram. Eng. Sci. Proc.* **16** (1995) 633.
14. B. E. YOLDAS, *J. Non-Cryst. Solids* **63** (1984) 145.
15. R. L. CALLENDER, C. J. HARLAN, N. M. SHAPIRO, C. D. JONES, D. L. CALLAHAN, M. R. WIESNER, R. COOK and A. R. BARRON, *Chem. Mater.* **9** (1997) 2418.
16. C. C. LANDRY, N. PAPPÈ, M. R. MASON, A. W. APBLETT, A. N. TYLER, A. N. MACINNES and A. R. BARRON, *J. Mater. Chem.* **5** (1995) 331.
17. R. L. CALLENDER, C. J. HARLAN, D. L. CALLAHAN, M. WIESNER, R. L. COOK and A. R. BARRON, *Ceramic Trans.* **87** (1998) 13.
18. A. KAREIVA, C. J. HARLAN, D. B. MACQUEEN, R. COOK and A. R. BARRON, *Chem. Mater.* **8** (1996) 2331.
19. C. J. HARLAN, A. KAREIVA, D. B. MACQUEEN, R. COOK and A. R. BARRON, *Adv. Mater.* **9** (1997) 68.
20. R. L. CALLENDER and A. R. BARRON, *J. Am. Ceram. Soc.* **83** (2000) 1777.
21. E. HECHT and A. ZAJAC, "Optics" (Addison-Wesley Publishing Company, Reading, MA, 1974).
22. "Handbook of Chemistry and Physics" 66th ed., edited by R. C. Weast (CRC Press, Boca Raton, Fl, 1985).
23. F. C. MONTGOMERY, H. H. STRECKET, R. O. HARRINGTON, J. L. KAAE, S. P. PAGUIO and D. R. WALL, *Mat. Res. Soc. Symp. Proc.* **180** (1990) 461.
24. T. K. GUPTA and J. VALENTICH, *J. Am. Ceram. Soc.* **54** (1971) 355.
25. M. K. CINIBULK and R. A. HAY, *ibid.* **79** (1996) 1233.
26. J. F. MANDELL, D. H. GRANDE, T. H. TSAING and F. J. MCGARRY, in "Composite Materials-Testing and Design," STP-893, edited by J. M. Whitney (American Society for Testing and Materials, Philadelphia, PA, 1986) p. 87.
27. P. BARTOS, *J. Mater. Sci.* **6** (1980) 3122.
28. R. J. KERANS, T. A. PARTHASARATHY, P. D. JERO, A. CHATTERJEE and N. J. PAGANO, *British Ceram. Trans.* **92** (1993) 181.
29. M. N. KALLAS, D. A. KOSS, H. T. HAHN and J. R. HELLMANN, *J. Mater. Sci.* **27** (1992) 3821.
30. D. B. MARSHALL, *J. Am. Ceram. Soc.* **67** (1984) C259.
31. M. D. THOULESS and A. G. EVANS, *Acta Metall. Mater.* **36** (1988) 517.
32. A. G. EVANS, *Mat. Sci Eng.* **71** (1985) 3.
33. M. K. BRUN and R. N. SINGH, *Adv. Ceram. Mater.* **3** (1988) 506.

Received 27 June 2000
and accepted 13 June 2001